Ensemble Prediction Methods based on Fast Growing Perturbations

Jorgen S Frederiksen, Mark A Collier
CSIRO Atmospheric Research

and

Andrew B Watkins
National Climate Centre
Bureau of Meteorology

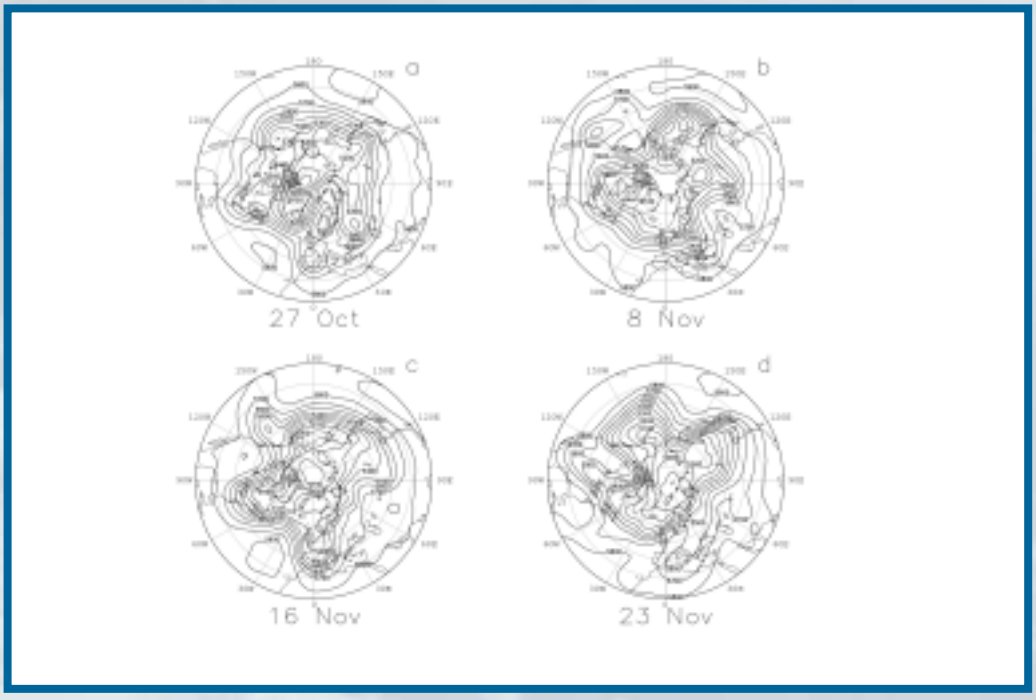

CSIRO
Atmospheric Research

CSIRO Atmospheric Research Technical Paper No.59

Ensemble Prediction Methods based on Fast Growing Perturbations

Jorgen S Frederiksen, Mark A Collier
CSIRO Atmospheric Research

and

Andrew B Watkins
National Climate Centre
Bureau of Meteorology

National Library of Australian Cataloguing in Publication Entry

Frederiksen, Jøorgen Segerlund.
Ensemble prediction methods based on fast growing perturbations.

ISBN 0 643 06655 1.

1. Weather forecasting. 2. Dynamic meteorology. I. Watkins, Andrew Bruce. II. Collier, Mark A. III. CSIRO. Division of Atmospheric Research. IV. Title. (Series : CSIRO Atmospheric Research technical paper (Online) ; 59).

551.51

Address and contact details: CSIRO Atmospheric Research
Private Bag No. 1, Aspendale Victoria 3195 Australia
Ph: (+61 3) 9239 4400 Fax: (+61 3) 9239 4444
Email: chief @csiro.au

CSIRO Atmospheric Research Technical Papers may be issued out of sequence

Ensemble Prediction Methods based on Fast Growing Perturbations

Jorgen S Frederiksen, Mark A Collier
CSIRO Atmospheric Research

and

Andrew B Watkins
National Climate Centre
Bureau of Meteorology

Abstract

An ensemble prediction scheme based on fast growing perturbations has been implemented for the CSIRO conformal-cubic and BMRC spectral general circulation models. The methodology uses an iterative procedure, based on an implicit linearization of the models, in which perturbations analogous to the leading Lyapunov vectors are obtained by a breeding method. Detailed comparisons of the skill of ensemble mean forecasts with control forecasts have been carried out for Northern Hemisphere initial conditions in October and November 1979. A particular focus has been the variability of forecast skill during the development, maturation and decay of the large-scale blocking dipoles that occurred in the major blocking regions over Europe, over the Gulf of Alaska, over the North Atlantic and as well over North America. On average, the ensemble mean forecast performs better than the control forecast for forecast times longer than 3 or 4 days. Average error growth curves in the two models are quite similar with the CSIRO conformal-cubic model ensemble generally performing slightly better than for the lower resolution BMRC spectral model. Both ensemble and control forecasts initiated twice daily exhibit considerable variability in forecast skill that is shown to be related to instability regimes of particular synoptic events. At a given forecast lead time, errors tend to be larger for forecasts validating when blocks are developing or decaying and smaller for mature blocks. The spread of ensemble member forecasts has been studied and related to likely forecast skill. Comparison of results from the CSIRO and BMRC models initialized with different analysis data sets (NCEP and ECMWF) has allowed the determination of the robustness of our findings.

1 Introduction

The inescapable uncertainty in specifying atmospheric initial states, due to chaos, means that weather prediction should be regarded as the problem of forecasting the probability density function of states in phase space or equivalently of determining the hierarchy of moments or cumulants of meteorological variables. Leith (1974) employed a second-order closure model in the context of two-dimensional turbulence to examine the growth of error spectra and their convergence towards the climatological variance associated with a typical atmospheric spectrum. His study was for the idealized problem of isotropic turbulence with zero mean fields. More recently, computationally tractable closures have been derived for general inhomogeneous barotropic flows over topography; these closures describe the time evolution of the mean fields and covariance and response function matrices (Frederiksen 1999; O'Kane and Frederiksen 2002). Currently however, the only feasible way of predicting the statistics of future atmospheric states using multi-level primitive equation general circulation models is by running an ensemble of forecasts from perturbed initial conditions.

It is generally agreed that the perturbed analyses should represent the fast growing errors that are present in initial conditions and that may be selectively bred by the data assimilation scheme (Toth and Kalnay 1993). There has been less agreement on how these perturbations should be characterised. At the European Centre for Medium Range Weather Forecasts (ECMWF) rotated singular vectors (SVs) in the total energy norm are used as the initial ensemble perturbations (Molteni et al. 1996; Palmer et al. 1998). At the National Centers for Environmental Prediction (NCEP), an iterative breeding method is used to generate ensemble perturbations that have been linked to leading Lyapunov vectors (LVs) (Toth and Kalnay 1993; 1997; Noone and Simmonds 1998; Kalnay 2002). Houtekamer et al. (1996) take the view that since the data assimilation scheme selectively breeds fast growing errors, one can use multiple analysis cycles to form ensemble perturbations.

Frederiksen and Bell (1990) argued that superpositions of fast growing normal modes would approximately characterize the instability and error growth in atmospheric flows over several days. A successful ensemble prediction scheme based on normal modes was implemented by Anderson (1996) for a low order dynamical system. Frederiksen (2000) showed that initial errors converge over time towards structures that can be represented by low order expansions in terms of the leading finite-time normal modes (FTNMs), which are the norm-independent eigenvectors of the tangent linear propagator. He suggests that it would therefore seem natural to be able to efficiently represent analysis error fields by a superposition of the leading FTNMs. Szunyogh et al. (1997) and Palmer et al. (1998) have also discussed the likely roles of different dynamical vectors in representing analysis errors.

In this report we describe the implementation and application of an iterative breeding method for ensemble prediction within two numerical weather prediction models viz., the CSIRO conformal-cubic model (McGregor and Dix 2001) and the BMRC spectral model (Hart et al. 1990; Frederiksen et al. 1996). Our primary aim is to examine the variability of forecast skill in different synoptic situations, focussing on the differences in skill between strong zonal flow situations and when mature blocks are present and as well on variability associated with the growth and decay phases of blocking.

In both hemispheres, numerical weather forecasts during the onset and decay of blocking frequently suffer from rapid loss of predictability (Bengtsson 1981; Noar 1983; Kimoto et al. 1992; Anderson 1993; Tibaldi et al., 1995; Molteni et al. 1996). Forecast errors during blocking transitions are also

limiting factors in producing successful medium and extended range forecasts (Colucci and Baumhefner 1992). Thus, examining the ensemble predictability during blocking regime transitions is of considerable practical importance for both short term and extended range forecasts.

It has been shown in a number of theoretical and numerical studies that instability processes of the large-scale flow play major roles in the development of blocking anomalies and in the growth of errors during blocking transitions (Frederiksen 1982, 1983, 2000; Simmons et al. 1983; Borges and Hartmann 1992; Anderson 1996; de Pondeca et al. 1998a, b; Li et al 1999). It has also been noted by Toth et al. (1997) that forecast errors arise primarily due to instabilities in the atmosphere rather than due to model deficiencies (Reynolds et al. 1994). In order to establish that the findings of our study are robust and are a reflection of the different instability regimes, depending on the synoptic situations, we compare results using two differently formulated models (CSIRO and BMRC GCMs) and with two different analysis data sets for the same times (NCEP and ECMWF). We focus on the sequence of dramatic blocking events that occurred over Scandinavia, over the Gulf of Alaska, over the North Atlantic and over North America during October and November 1979.

The plan of this report is as follows. In Section 2, we present brief descriptions of the CSIRO conformal-cubic and BMRC spectral models which are used in the control and ensemble predictions. Section 3 presents a summary of the ensemble prediction methodology used and the relation between the breeding method and four-dimensional data assimilation schemes. In Section 4, we describe the synoptic situations associated with the major blocking events over Scandinavia, over the Gulf of Alaska, over the North Atlantic and over North America that occurred during October and November 1979. The vertical and horizontal structures of the bred ensemble perturbations in the CSIRO and BMRC numerical weather prediction models are examined in Section 5.

In Section 6, we examine the growth of ensemble and control 500 hPa Northern Hemisphere zonal velocity errors (averaged between 20° and 90°N). We study these errors for forecasts in the two models started each 12 hours between 0000 UTC on 11 October and 1200 UTC on 21 November 1979. We also calculate averages over this time interval and present similar diagnostics for 500 hPa geopotential heights. In Section 7, we focus on error growth of ensemble and control forecasts in the Atlantic sector between 0° and 60°W and relate the root-mean-square (RMS) errors to the synoptic situations in this region and in the regions upstream and downstream. In Section 8, we examine in more detail ensemble mean forecasts of 500 hPa geopotential heights, spread of the ensemble members and error growth during the development of the four major blocking events. Our conclusions are detailed in Section 9.

2 General circulation model details

The forecast experiments performed in this technical report have been carried out with two numerical weather forecast models developed at CSIRO and BMRC. The CSIRO GCM is a semi-Lagrangian model which uses a novel conformal-cubic grid; in all our simulations we use a C48 conformal-cubic grid, as in Fig.2 of McGregor and Dix (2001), with an average resolution of about 200 km, and employ 18 vertical sigma levels. The model incorporates a comprehensive list of physical parameterizations as described by McGregor and Dix (2001) including representations for long and shortwave radiation, interactive cloud distributions, cumulus and shallow convection schemes and evaporation of rainfall. It includes a stability-dependent boundary layer and vertical diffusion, Smagorinsky deformation-based

horizontal diffusion (Smagorinsky et al. 1965) and a vegetation-canopy scheme with prognostics for soil temperatures and soil moisture.

The BMRC GCM is a spectral model employing spherical harmonic basis functions. In all simulations we use an R31 resolution, in which the rhomboidal truncation wave number is 31, and use 9 vertical sigma levels. The R31 resolution corresponds approximately to a grid spacing of 330 km at midlatitudes. The BMRC model also includes a comprehensive list of physical parameterizations as described by Hart et al. (1990) and Frederiksen et al. (1996). These cover most of the processes described for the CSIRO GCM but are in general formulated somewhat differently. In particular, the BMRC model employs a Laplacian horizontal diffusion with a diffusion coefficient of 2.5×10^5 m^2 s^{-1} and is applied only to waves with a total wavenumber $n \geq 31$. The current version of the BMRC model has fixed zonally averaged cloud amounts.

3 Ensemble prediction methodology

As discussed in the introduction, a number of successful methods of generating perturbations for ensemble predictions have been proposed and applied both in research and operational modes. Currently there is no agreement upon which method is preferable from theoretical and practical points of view. However, there appears to be consensus that in order to obtain improved forecasts with ensemble prediction methods it is necessary to use perturbations which have similar structures to the fast growing errors present in initial analyses. Toth and Kalnay (1993) argue that current four-dimensional (space-time) data assimilation schemes, although far superior to using persistence or climatology to fill data-poor regions, cause the breeding of fast growing perturbations. Typically, in an operational data assimilation cycle, a six hour forecast is made from initial conditions determined by a previous analysis. The next analysis is then calculated as a weighted combination of the six-hour forecast and observations collected during a six-hour window centred on the analysis time, with the weighting determined geographically by the statistical reliability of the observations. Repetition of the process for subsequent analyses, four times every day, decreases the total error in the analysis but increases the ratio of the fast growing errors to the total error.

There is less agreement about what types of perturbations are most likely to efficiently represent analysis error (Szunyogh et al. 1997; Palmer et al. 1998; Frederiksen 1997, 2000). Superpositions of rotated singular vectors (SVs) in the total energy norm are used to perturb the control analyses and form the initial ensembles at the ECMWF (Molteni et al. 1996; Palmer et al. 1998). At NCEP a 'breeding' method is used to generate the initial ensembles and the bred perturbations have been linked to the leading Lyapunov vectors (LVs) (Toth and Kalnay 1993; 1997). Houtekamer et al. (1996) use multiple analysis cycles to generate their initial ensembles. Frederiksen (2000) has shown that initial errors contract onto a low dimensional phase space spanned by the leading FTNM, which are the norm-independent eigenvectors of the tangent linear propagator. Indeed, after a few days, different fast growing perturbations, such as leading singular vectors, Lyapunov vectors or FTNMs, tend to evolve towards very similar structures (Frederiksen 2000).

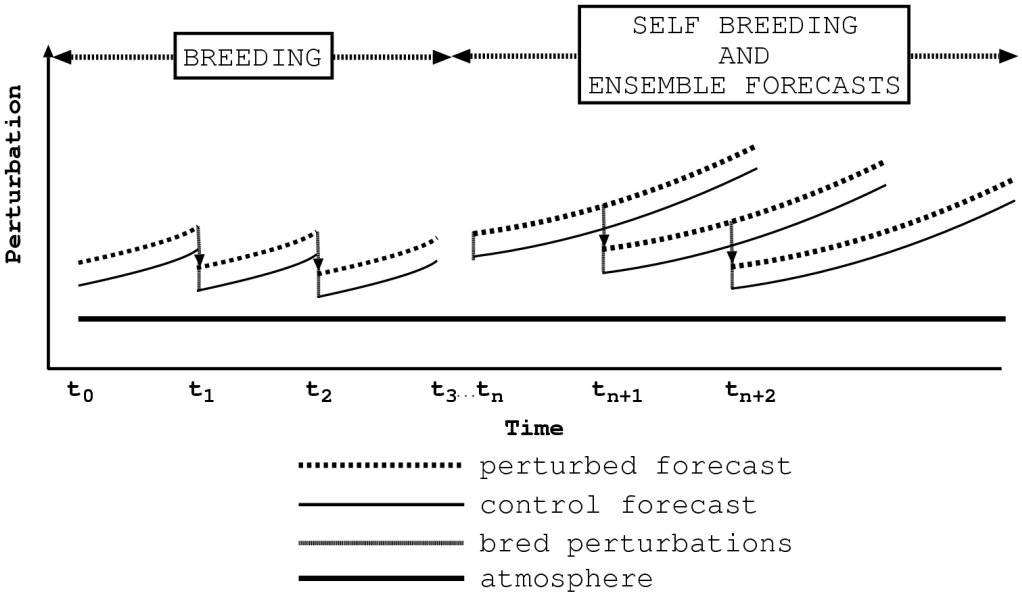

Figure 1 Schematic showing the breeding cycle for generating perturbations followed by ensemble forecasts which maintain their own breeding cycle, known as self-breeding. See text for a detailed explanation.

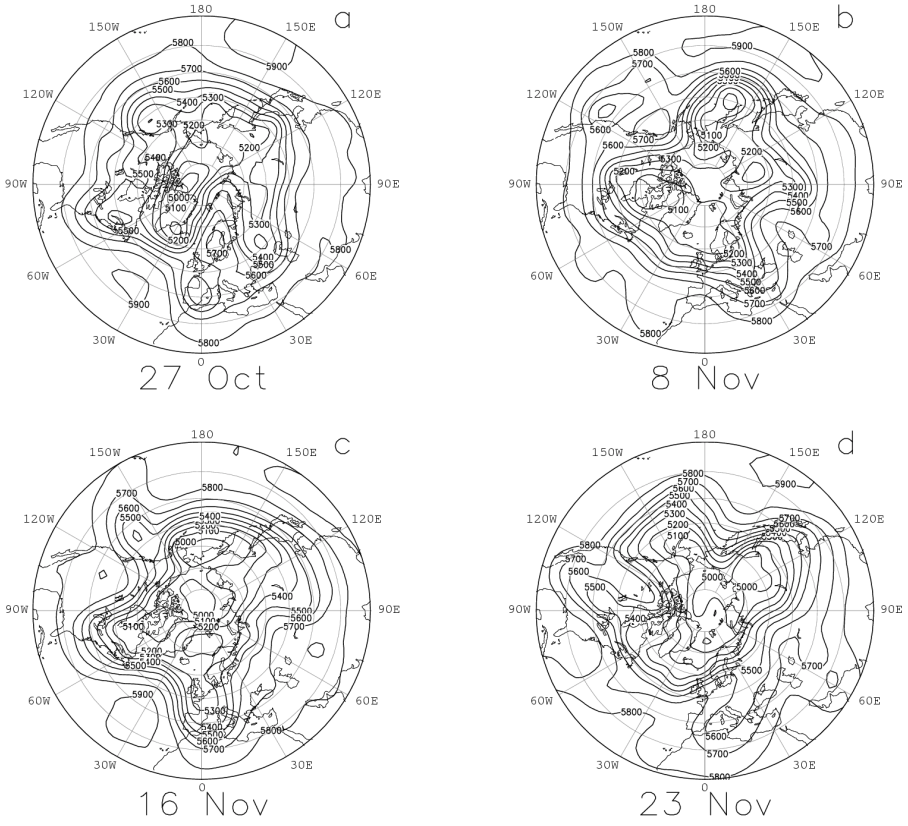

Figure 2 Northern Hemisphere 500 hPa geopotential heights (m) based on NCEP analyses for 0000 UTC on (a) 27 October, (b) 8 November, (c) 16 November and (d) 23 November 1979.

The theoretical advantages of using different dynamical vectors (SVs, LVs or FTNMs) as ensemble perturbations have been discussed in some detail by Szunyogh et al. (1997), Palmer et al. (1998) and Frederiksen (1997, 2000). In this study we shall employ an iterative breeding method (Toth and Kalnay 1993, 1997) primarily because it is a successful method which is relatively easy to implement and computationally relatively cheap. The version of this method that we employ is summarized in the schematic in Fig.1. It consists of a period of 10 days of breeding of perturbations starting at the beginning of October 1979 followed by a period of self-breeding and 10 day ensemble forecasts starting at 0000 UTC on 11 October and finishing at 1200 UTC on 21 November 1979.

During the breeding period a specified small perturbation is added to the analysis and 12-hour forecasts are performed from both the perturbed and unperturbed (control) initial conditions. The difference between the 12-hour perturbed and control forecasts is then scaled to have the same root-mean-square (RMS) magnitude as the initial perturbation and is added to the subsequent 12-hour analysis. Again 12-hour forecasts are performed from both the new perturbed and unperturbed analysis and the process is repeated until the end of the 10-day breeding period. The breeding methodology corresponds essentially to an implicit linearization of the nonlinear dynamics about the time-dependent analyses and would with time result in the bred perturbation converging to the leading Lyapunov vector were it not for stochastic effects associated with the convective parameterizations in the numerical weather prediction models.

After the 10-day breeding period 10-day forecasts are performed from both the perturbed and control analyses, as indicated in the schematic. As well 10-day forecasts are performed from the control analyses perturbed by bred perturbations with opposite signs. Twelve hours into the 10-day forecasts, the difference between the 12-hour perturbed and control forecast is scaled to the standard RMS magnitude and added to the subsequent 12-hour analysis. Again 10-day forecasts are performed from both the new perturbed and unperturbed analyses (and from the analysis perturbed by the bred perturbation with opposite sign) and the process is repeated until 1200 UTC on 21 November.

In practice, we perform eight separate breeding cycles starting from 8 different perturbations over the first 10 days. The self-breeding is also performed for 8 different perturbations with the ensemble forecast consisting of 16 forecasts employing the 8 initial bred perturbations and 8 initial identical perturbations with opposite signs. This ensures that the ensemble mean forecast starts from the same initial condition as the control. This method of using 2n paired perturbations of opposite signs from n independent breeding cycles appears to be superior to using 2n independent bred perturbations (with their mean subtracted from each perturbation) (Toth and Kalnay 1997).

4 Synoptic situations

We examine the performance of the ensemble prediction method described in Section 3 for initial conditions taken from the period between 0000 UTC on 11 October 1979 and 1200 UTC on 21 November 1979. We have focussed on this interval because it was a time of large-scale Northern Hemisphere blocking in the major blocking regions over Europe, over the Gulf of Alaska, over the North Atlantic Ocean and as well over North America. As this time interval coincides with the First Global Atmospheric Research Program Global Experiment (FGGE), observations are of the highest quality. Ensemble and control forecasts have been commenced every 12 hours during this time interval. This sequence of developing, mature and decaying blocks alternating with times of strong zonal flows

seems an interesting period for studying the variability of predictability and for examining the differences between ensemble and control forecasts.

Some of the major blocks which occurred in October and November 1979 are shown in Figure 2. The 500 hPa heights taken from NCEP analyses at 0000 UTC depict the mature phase of the large-scale Scandinavian block on 27 October (Fig.2a), the Gulf of Alaska block on 8 November (Fig.2b), the North Atlantic block on 16 November (Fig.2c) and the North American block on 23 November (Fig.2d). The European block started developing around 21 and 22 October over the UK and intensified to form the large-scale high-low dipole block on 27 October with the high centred over Scandinavia and the low over Spain as depicted in Fig.2a. These centres subsequently decayed and moved downstream in late October. In early November, the flow over the Gulf of Alaska became more diffluent with the blocking ridge developing rapidly around 5 November and forming the cut-off high-low dipole pair on 8 November shown in Fig.2b. The Gulf of Alaska block weakened between 10 and 12 November and was followed by downstream development of a blocking high over the Atlantic Ocean around 13 and 14 November. The high-low dipole shown in Fig.2c on 16 November subsequently decayed around 17 and 18 November. Around 20 November ridging again occurred over the Gulf of Alaska leading to diffluent flow around a large-scale high-low dipole block over North America on 23 November (Fig.2d). This block persisted until 26 November and then decayed.

5 Bred perturbations

The ensemble prediction methodology described in section 3 results in the convergence of fairly arbitrary initial perturbations towards bred vectors, which have fairly similar large-scale features after about 10 days. This has been tested by computing pattern correlations between the different bred vectors, for both the CSIRO and BMRC models, all finishing on a given day. Bred vectors generated within different models, however, do differ somewhat as discussed in detail below. Within a given model the main difference between bred vectors for breeding times longer than about 10 days is due to the stochastic element introduced by the convection schemes in the models as discussed by Toth and Kalnay (1993, 1997).

The vertical and horizontal structures of geopotential heights for typical bred perturbations on days of particular interest in this study (27 October, 8 November and 16 November) are summarized in Figs 3 and 4. Figure 3 shows that for both the CSIRO and BMRC models the bred perturbations have fairly constant magnitudes throughout the troposphere with in some cases larger amplitudes at the surface. The structures of the perturbations are in fact largely equivalent barotropic throughout the upper troposphere and more baroclinic near the surface. Throughout this study the Northern Hemisphere geopotential height bred perturbations are normalized to 15 m at 500 hPa. This has been found empirically to be nearly optimal for increasing the skill with ensemble forecasts (see also Toth and Kalnay 1997). Figures 4a and b show the 500 hPa bred perturbations in the CSIRO and BMRC models on 27 October. We note the pair of low-high and high-low dipoles stretching across Europe for both models with different structures in the rest of the hemisphere.

On 8 November the 500 hPa bred perturbations in Figs 4c and d have wave trains extending across the North Pacific and into the Gulf of Alaska and across America. For the BMRC model in particular, the wave train shown in Fig.4d has some qualitative similarities to the finite-time normal mode on 8 November shown in Fig.4d of Frederiksen (1997) (but with opposite arbitrary sign). This latter structure was obtained as the leading finite-time normal mode for the period 31 October to 16

November within a two-level quasi-geostrophic tangent linear model. By 8 November the FTNM would be close to converging towards the leading Lyapunov vector (Frederiksen 2000). These results are consistent with the ideas of Toth and Kalnay (1993, 1997) that the bred vectors are the nonlinear analogues of the leading Lyapunov vector, modified somewhat in their smaller scales by the stochastic effects of the convection parameterizations.

Figs 4e and f show the CSIRO and BMRC model bred perturbations on 16 November. Both perturbations, but in particular the CSIRO model perturbations, have high low-dipoles near the Greenwich meridian similar to the leading evolved singular vector (SV) and leading FTNM shown in Figs 8a and b of Frederiksen (2000) (but with opposite arbitrary sign). As discussed there, these structures in turn have essentially converged to the leading Lyapunov vector for the period 16 October to 16 November. Outside the key region of the North Atlantic where the large scale blocking occurs on 16 November (Fig.2c) there are, however, differences in the structures of the bred perturbations in the two GCMs and in comparison with the dynamical vectors shown in Figs 8a and b of Frederiksen (2000).

It is clear that the bred perturbations in both GCMs have major centres in the regions of dominant instability (as determined in the studies of Frederiksen 1997, 1998 and 2000) but also appear to mix in some of the nonleading modal structures, presumably due to nonlinearity and the presence of stochastic effects due to convection.

6 Hemispheric ensemble mean forecast results

As discussed in Section 3, in all our ensemble forecasts we use 16 paired perturbations obtained by the breeding method with the two perturbations in each of the eight pairs having opposite signs. Toth and Kalnay (1997) have discussed the advantages of the perturbations having opposite signs so that when added to the analysis, the initial ensemble mean is identical to the analysis. In our experiments, we have examined error growth in terms of 500 hPa geopotential height, zonal velocity, meridional velocity and temperature. We have also examined some surface fields including surface pressure and temperature. In order to minimize differences in model forecast results and analyses, which have been derived based on other data assimilation systems and models viz., NCEP or ECMWF, we find it most useful to do some of our comparisons using fields such as the 500 hPa zonal wind. This field is directly carried in the prognostic equations of both the CSIRO and BMRC models. Derived fields such as geopotential heights that involve an integration from the surface, may be more influenced by differences in topography and surface processes between the models used here and the NCEP or ECMWF models.

In Figs 5a and b we show for the CSIRO and BMRC models the 500 hPa Northern Hemisphere RMS zonal wind errors (between 20° and 90°N) for the ensemble mean and control forecasts averaged between 0000 UTC on 11 October and 1200 UTC on 21 November 1979. We note that for forecasts longer than about 3 days the average errors of the ensemble mean forecasts are lower than for the control forecasts. Quite similar results are obtained in terms of the 500 hPa geopotential height as shown for the BMRC model in Fig.6. For both BMRC and CSIRO models 500 hPa geopotential height errors in m are typically ten times 500 hPa zonal velocity errors in m s^{-1} for forecast times longer than 4 days. This relationship which is evident from Figs 5 and 6 for average forecast errors also applies in good measure for errors on a particular day. Our results for average forecast errors are broadly comparable with the results of Molteni et al. (1996) for winter (their Fig.13a) in which they used ensemble perturbations based on rotated singular vectors in the total energy norm.

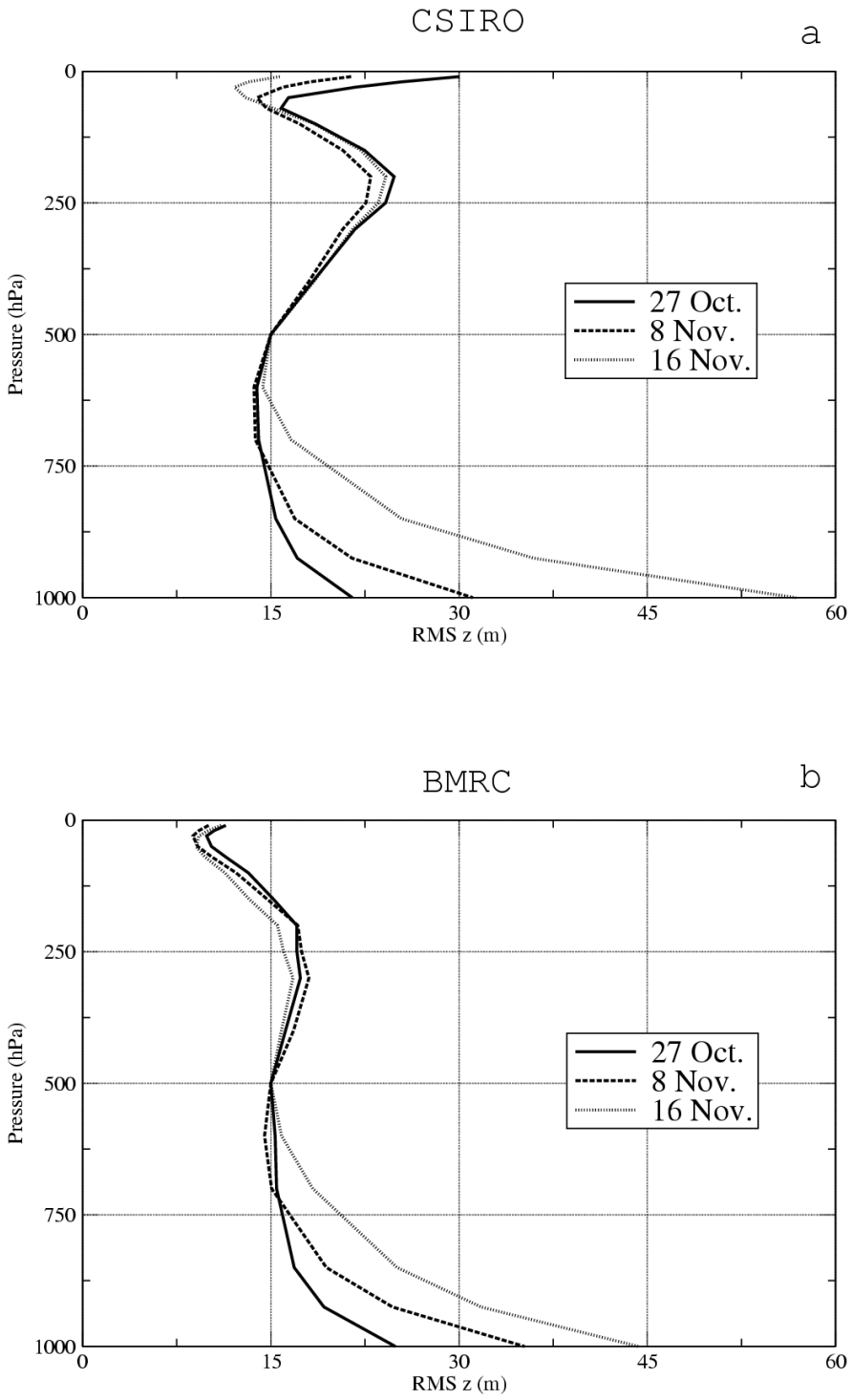

Figure 3 Vertical structures of Northern Hemisphere RMS geopotential height (m) between 20° and 90°N for bred perturbations at 0000 UTC on 27 October, 8 November and 16 November 1979 for (a) CSIRO and (b) BMRC models.

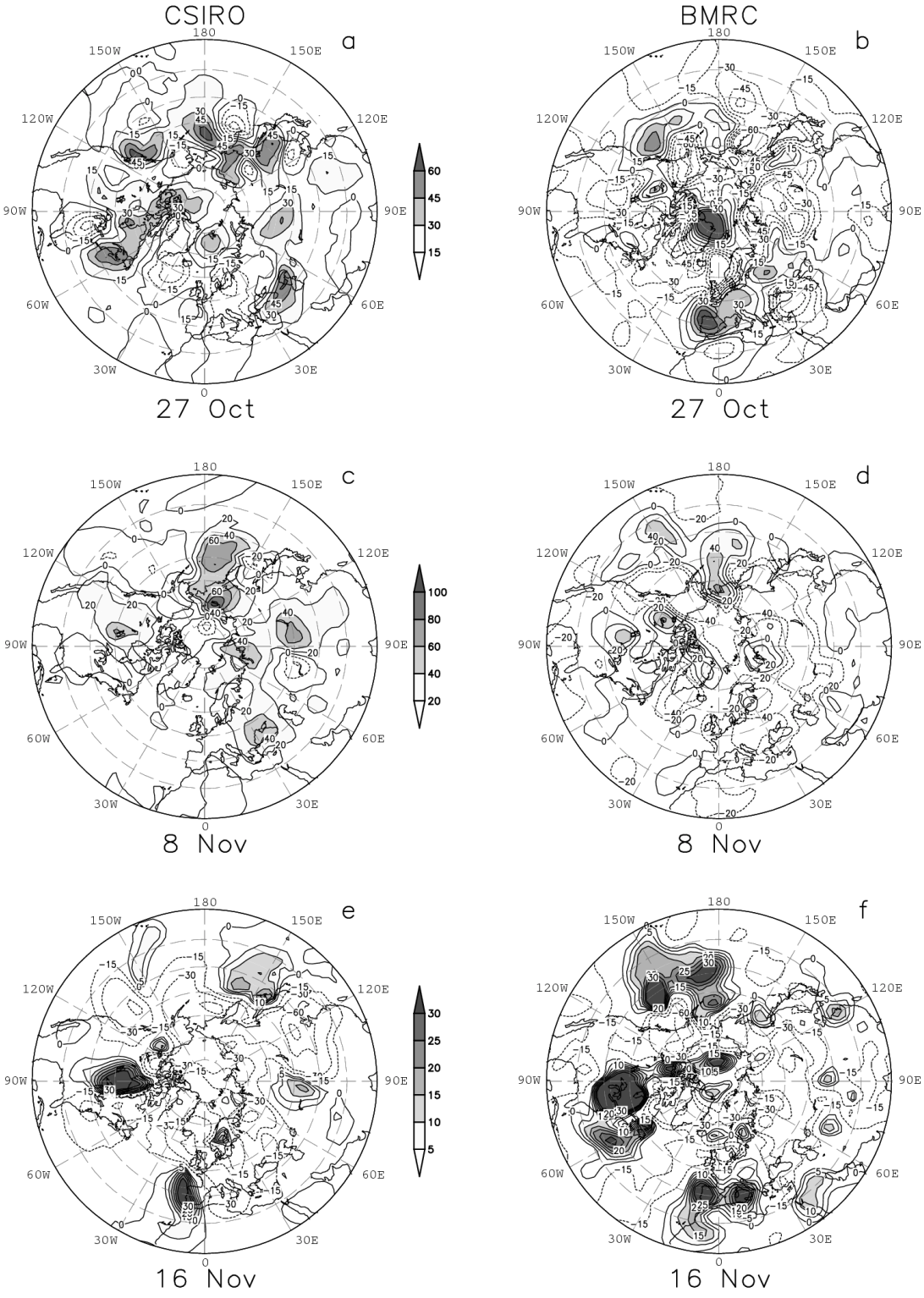

Figure 4 Horizontal structures of Northern Hemisphere 500 hPa geopotential height (m) for bred perturbations at 0000 UTC on 27 October, 8 November and 16 November 1979 for CSIRO (left column) and BMRC (right column) models.

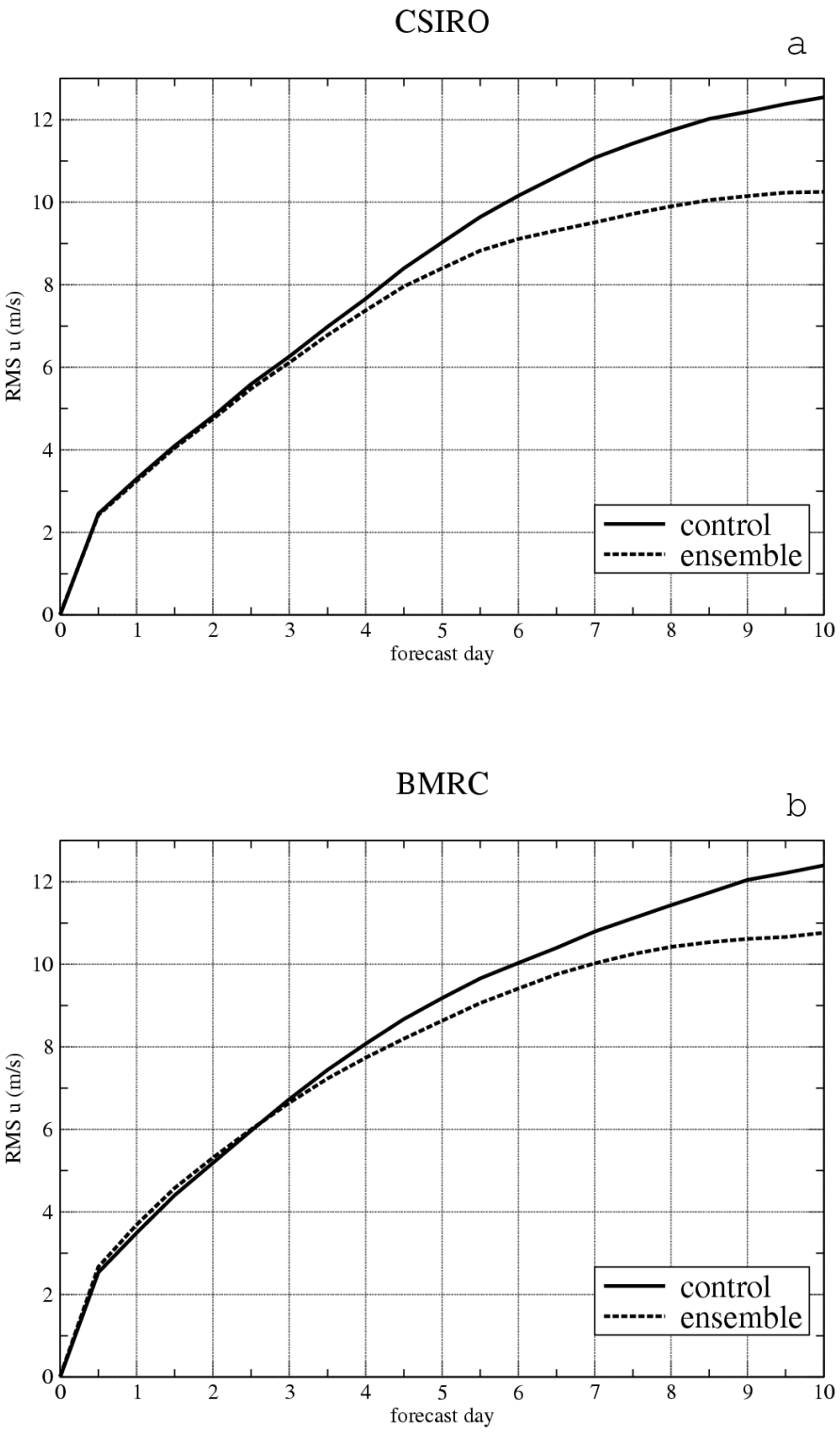

Figure 5 Northern Hemisphere RMS errors of 500 hPa zonal wind (m s-1), averaged between 0000 UTC on 11 October and 1200 UTC on 21 November 1979, for ensemble mean and control forecasts with the CSIRO and BMRC models.

The average error growth results shown in Figs 5a and b for the CSIRO and BMRC models have been determined from the twice daily 10 day forecast error results shown in Figs 7 and 8 respectively. From Figs 7 and 8 for the CSIRO and BMRC GCMs we see that although the average of the ensemble mean forecasts is superior to the average of the control forecasts after a few days, there is considerable variability in the skill with the control forecast occasionally beating the ensemble mean as expected. We also note from Figs 7a and b and 8a and b that there is also considerable variability in the skill of both the ensemble mean and control forecasts. We shall find that this variability can be related to particular synoptic events, particularly the development, maturation and decay of blocks, and that it is more distinct when the RMS errors are calculated over smaller 60° longitude sectors (as in section 6) that are particularly affected by the synoptic events. Even in the hemispherically (20°-90°N) averaged RMS results shown in Figs 7a and b and 8a and b we see some evidence of higher control and ensemble errors for forecasts ending around 25 October when the European block is forming and lower errors for forecast ending around 30 October which covers the mature period of the European block. Similarly errors tend to be larger when the Gulf of Alaska block is developing around 5 November and smaller when it is in the mature phase around 8 November. Again errors tend to be smaller when the North Atlantic block is mature, around 16 November, and when the North American block is mature, around 23 November, and are larger a few days earlier when these blocks are developing.

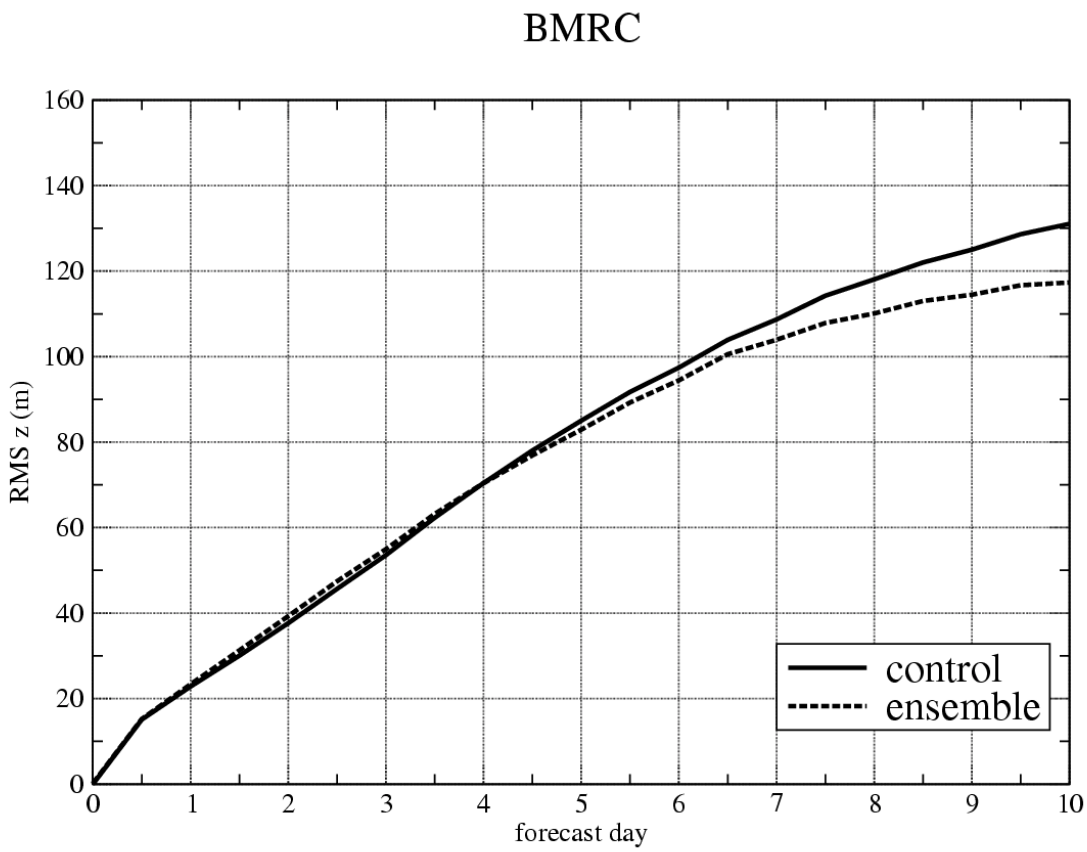

Figure 6 As in Figure 5 for RMS errors of 500 hPa geopotential height (m) in the BMRC model.

Despite the fact that the results in Figs 7 and 8 have been obtained with different models (CSIRO and BMRC) initialized and validated against different data sets (NCEP and ECMWF), the Hovmoeller diagrams of 10-day forecast errors against analysis time show many similarities for the respective ensemble, control and control-ensemble. This similarity may be quantified by pattern correlations of the CSIRO and BMRC model Hovmoeller diagrams. These pattern correlations have the values of 0.996 for the ensemble errors, 0.994 for the control errors and 0.650 for the control-ensemble. If one subtracts the time mean errors (between 0000 UTC on 11 October and 1200 UTC on 21 November) from Figs 7 and 8 then pattern correlations between the time mean anomalies are 0.628 for ensemble errors and 0.455 for control errors. These results indicate that not only is the average growth of errors similar in the CSIRO and BMRC models but so is the variability of error growth depending on the synoptic situation particularly for ensemble forecasts.

Next, we examine in more detail the skill and spread of ensemble forecasts focusing on periods relevant to the European and Gulf of Alaska blocks. The three panels in Fig.9a show the error growth of the control and ensemble simulations for the 10-day period starting on 17 October for the CSIRO model, the corresponding error growth of the individual ensemble members, which provides a measure of the spread of the forecasts, and the error growth of the control and ensemble simulations for the BMRC model. The BMRC model tends to have slightly less spread than the CSIRO model (not shown). For this particular case there is good agreement between the CSIRO and BMRC errors for both the controls and ensembles. It tends to be the case that there is a general similarity in the improvement in forecasts with the ensemble methodology for both models although, as seen from Figs 7 and 8, on occasions the two models produce qualitatively different results. One particular example is for the 10-day period starting on 22 October for which the ensemble forecast in the CSIRO model is significantly better than the control after 25 October, while in the BMRC model there is little difference between the two with the control actually being slightly better than the ensemble in the last few days of the forecast (not shown).

Fig.9b shows the same panels as in Fig.9a but for the 10-day period starting on 31 October and covering the development and maturation of the Gulf of Alaska block. The panels in Fig.9c are again for the same period as in Fig.9b but with the RMS error calculations restricted to the sector 20°-90°N and 0°-60°W covering the North Atlantic region where the major storm track occurs. In both Figs 9b and 9c, we see relatively rapid error growth as the Gulf of Alaska block starts to form and this occurs in both the control and ensemble results, with the ensembles superior to the controls after 4 November. Particularly evident in the results for the North Atlantic sector is the recovery of the forecast accuracy once the block has formed and is maturing.

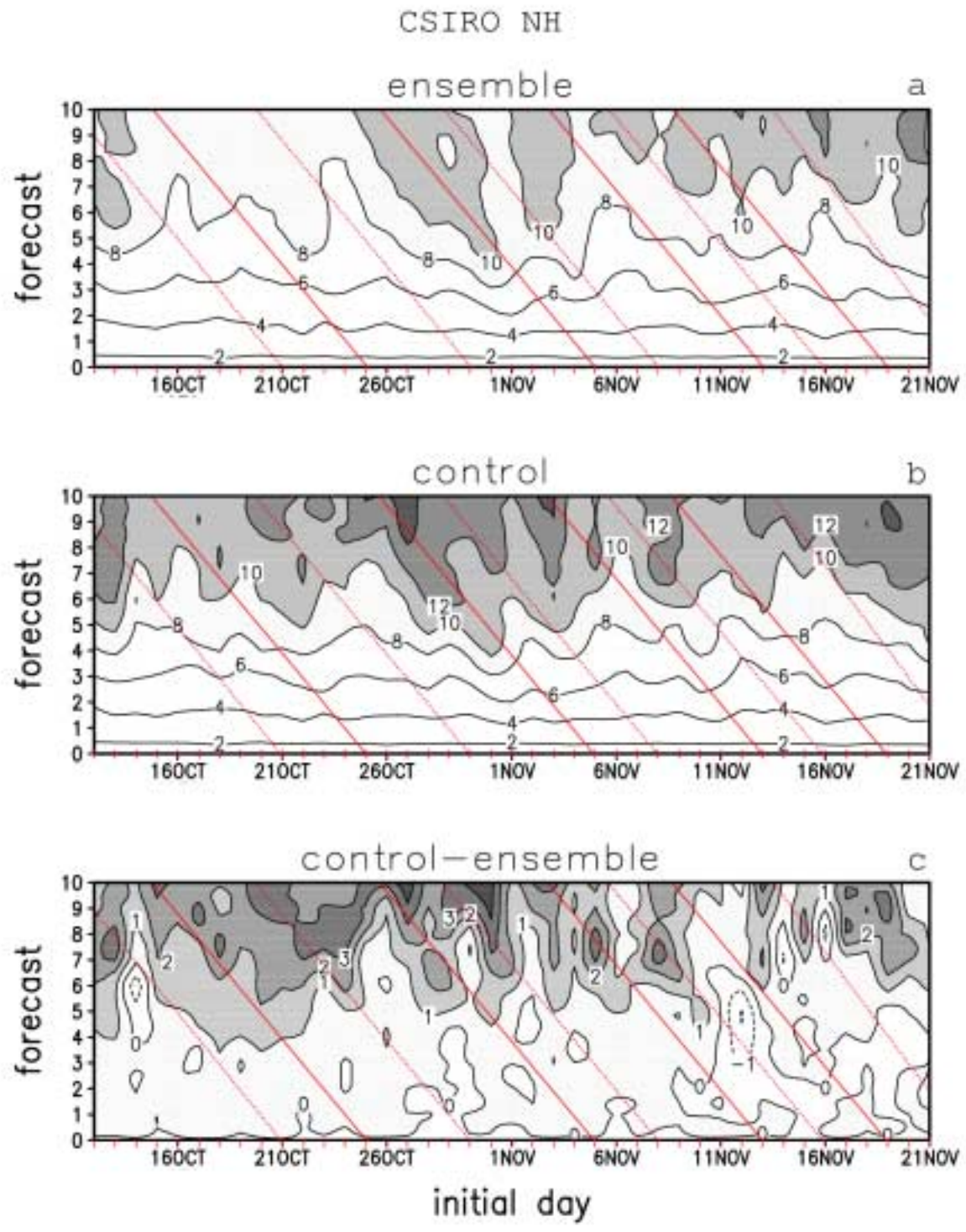

Figure 7 Northern Hemisphere RMS errors of 500 hPa zonal wind (m s-1) in 10 day forecasts initiated every 12 hours between 0000 UTC on 11 November and 1200 UTC on 21 November 1979 and for ensemble, control and control-ensemble in the CSIRO model. The tick marks on both axes denote a day.

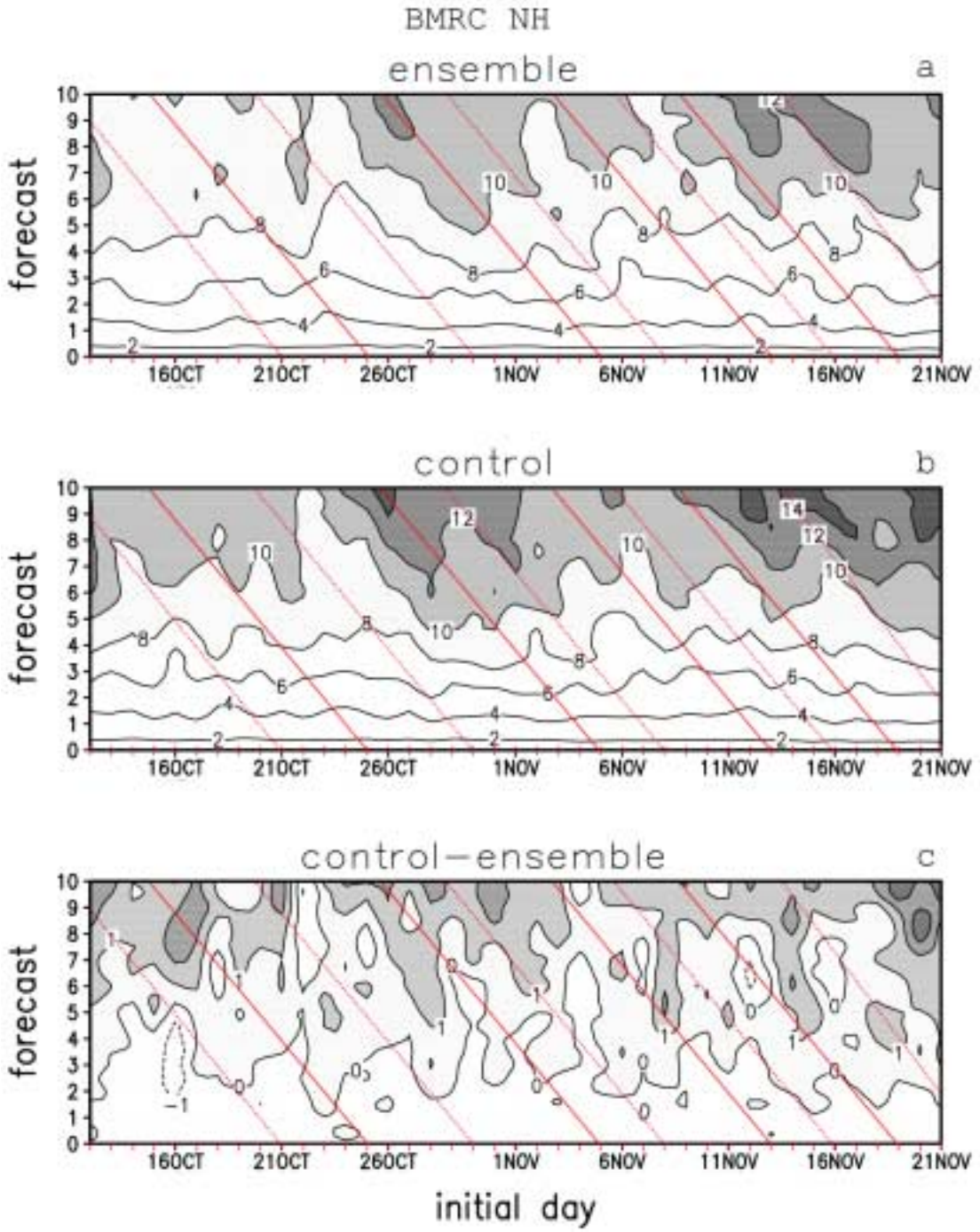

Figure 8 As in Figure 7 for the BMRC model.

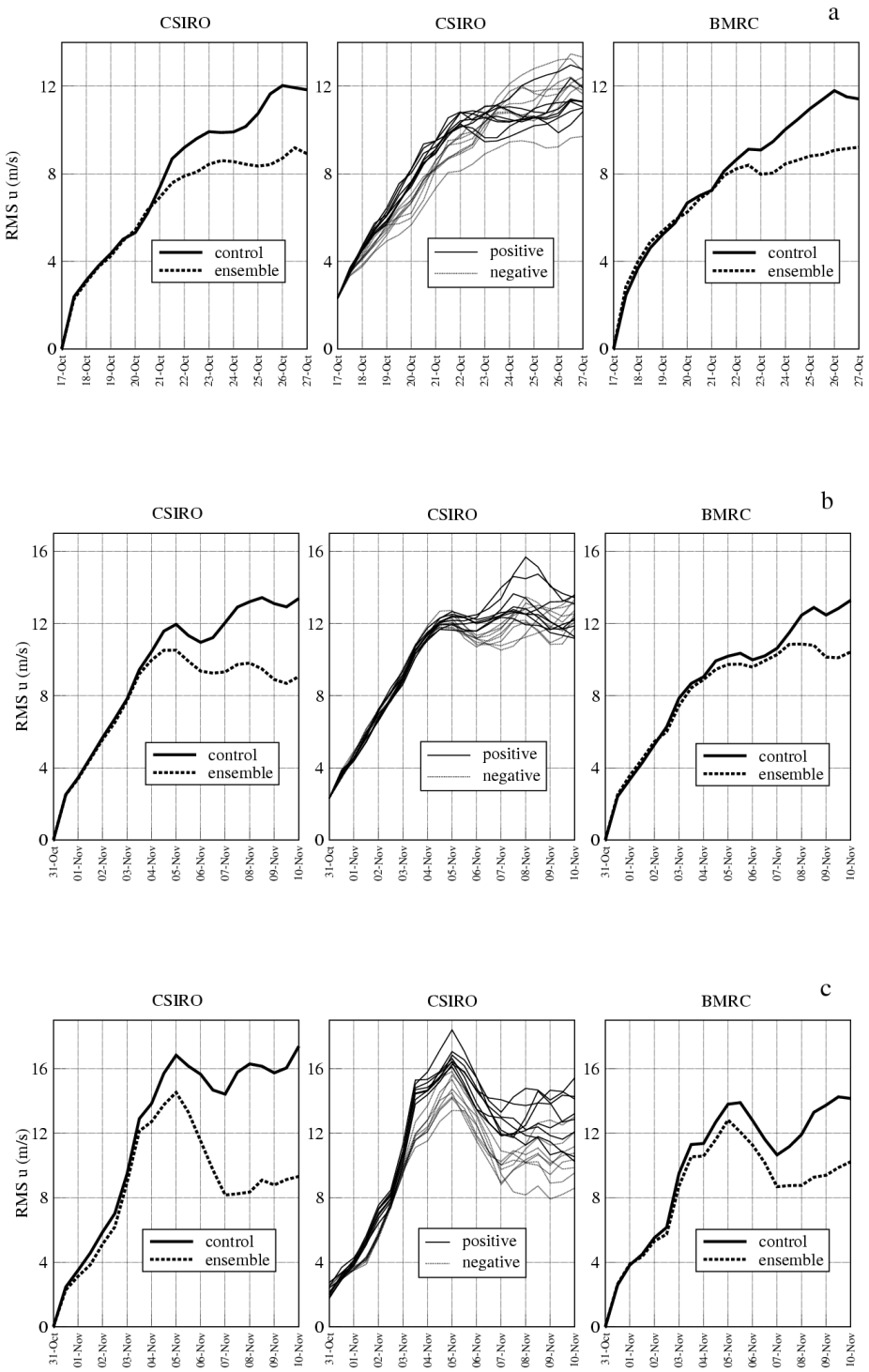

Figure 9 Northern Hemisphere RMS errors of 500 hPa zonal wind (m s-1) in 10 day ensemble mean and control forecasts in CSIRO and BMRC models initiated at 0000 UTC on (a) 17 October and (b) 31 October. Also shown are the corresponding errors associated with the 16 ensemble members. Shown in (c) are the same results as in (b) but for the North Atlantic sector.

7 Forecast results for the Atlantic sector

As noted in Fig.9c, examining the error growth of ensemble and control forecasts in particular sectors can highlight aspects of the relationship between developing and mature blocks and error growth. We have therefore carried out studies like those described in Section 5 but focusing on 60° longitude sectors of the Northern Hemisphere extratropics (20°-90°N) where the different blocks form. In fact , the development of a block or the presence of a mature block in a given sector affects not only the error growth in the sector but tends to have a similar effect on sectors both upstream and downstream. For this reason, and because the Atlantic sector is a region for a major Northern Hemisphere storm track, we focus here on the sector 20°-90°N, 0°-60°W.

Figs 10 and 11 show the RMS zonal wind errors of CSIRO and BMRC ensemble, control and control-ensemble 10 day forecasts started every 12 hours for the Atlantic sector. These results should be compared with the corresponding hemispherically averaged results shown in Figs 7 and 8. We note that in the Atlantic sector the variability of error amplitudes depending on the synoptic situation is considerably larger than for the hemispherically averaged results, as might be expected. The signatures of the life cycle of the four blocks summarized in Section 3 are particularly clear in the control and especially ensemble errors shown in Figs 10 and 11. Forecasts on diagonals ending on 25 October, 5 November, 13 November and 19 November, when the blocks in the respective European, Gulf of Alaska, Atlantic and North American regions are rapidly developing, tend to have relatively large errors for a given forecast time. In contrast, when the blocks have reached their mature phase, on the 30 October, 8 November and 23 November, forecast errors are relatively smaller than average for a given forecast time. This is consistent with the notion that errors grow rapidly when dynamical development is rapid (Frederiksen and Bell 1990) and are suppressed in the presence of large-scale equivalent barotropic waves (Frederiksen 1978; Colucci and Baumhefner 1992). The less intense block on 16 November appears to have a less systematic effect.

Again, we may quantify the similarities of the error growth shown in the Hovmoeller diagrams for the Atlantic sector in the CSIRO and BMRC models. These pattern correlations are 0.983 for ensemble errors, 0.980 for control errors and 0.412 for control-ensemble. The pattern correlations between time mean anomalies are 0.611 for ensemble errors and 0.540 for control errors. These results are quite comparable with the findings for the whole Northern Hemisphere extratropics discussed in section 7.

8 Ensemble forecasts and error growth during block development

Next, we examine how forecast errors and forecast spread become structurally organized in particular geographical regions, focussing on cases of block development. Figs 12a and b show the ensemble mean forecast of 500 hPa geopotential height in the CSIRO GCM for forecasts starting on 26 and 24 October respectively and valid for 27 October 1979. Both the 3-day and 1-day forecasts capture the block formation over Scandinavia but in the 3-day forecast it is somewhat too weak. This may be seen from a comparison of Fig. 12b with Fig.2a or from the error field of the 3-day CSIRO model ensemble forecast shown in Fig.13a. The corresponding 1-day error field (not shown) is of smaller scale and about a third the magnitude. This is also the case for 1-day error fields corresponding to the 3-day CSIRO model error fields in Figs 13c and 13e. Again the low over Spain is captured in the 1-day forecast but is too weak in the 3-day forecast. The 1-day forecast provides a better prediction of the structure and amplitude of the associated low over Asia Minor. These features of the 1- and 3-day

forecasts, as seen by comparing Figs 12a and b with the NCEP analyses in Fig.2a, and from Fig.13a, are reflected in the 1- and 3-day standard deviations of the 16 CSIRO model forecasts making up the ensembles.

The standard deviations measuring the spread of the individual forecasts in the ensembles are depicted by the shading in Figs 12a and b. We note the considerably large standard deviations associated with the 3-day forecast compared with the 1-day forecast, with considerable spread in the region of the low over Asia Minor in the 3-day forecast and also evident in the 1-day forecast. Again, there is significant spread in the blocking region over Scandinavia, particularly in the 3-day forecast, and in the region of the low over Spain. As well we notice the wave train of variable standard deviations extending across the major storm track in the Pacific and across North America. This variability in the forecasts appears to be associated with the development of baroclinic transients in the major storm track. As expected, the spread associated with baroclinic transients is larger in the 3-day forecast but still quite distinct in the 1-day forecast. We also note the variability in the forecasts associated with the development of the lows in the Arctic region. These features of the spread of ensemble member forecasts are also seen in the error field in Fig.13a indicating the close connection between the two.

We note from Figs 13a and 13b that the 3-day error fields for the CSIRO model ensemble and the BMRC model ensemble have quite similar structures, particularly in the regions of large amplitude. This is also the case for the other time periods (Figs 13c and 13d and Figs 13e and 13f) shown in Fig.13. Here the BMRC model 3-day error fields are the differences between the BMRC ensembles and the ECMWF analysis. Again the general relationships between ensemble spread and error structure found for the CSIRO model forecasts apply to the BMRC model forecasts for each of the three periods in Fig.13.

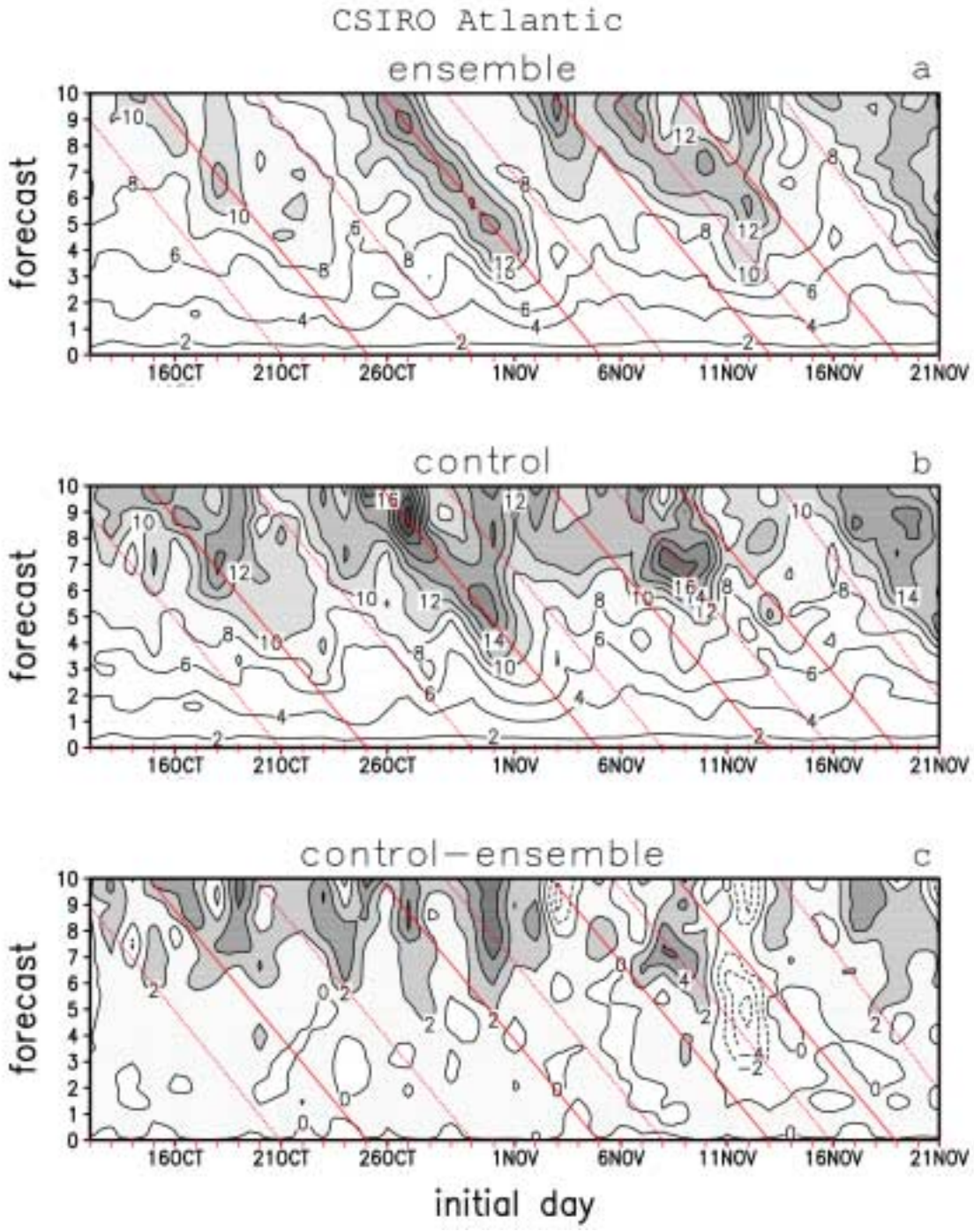

Figure 10 As in Figure 7 but for the North Atlantic sector.

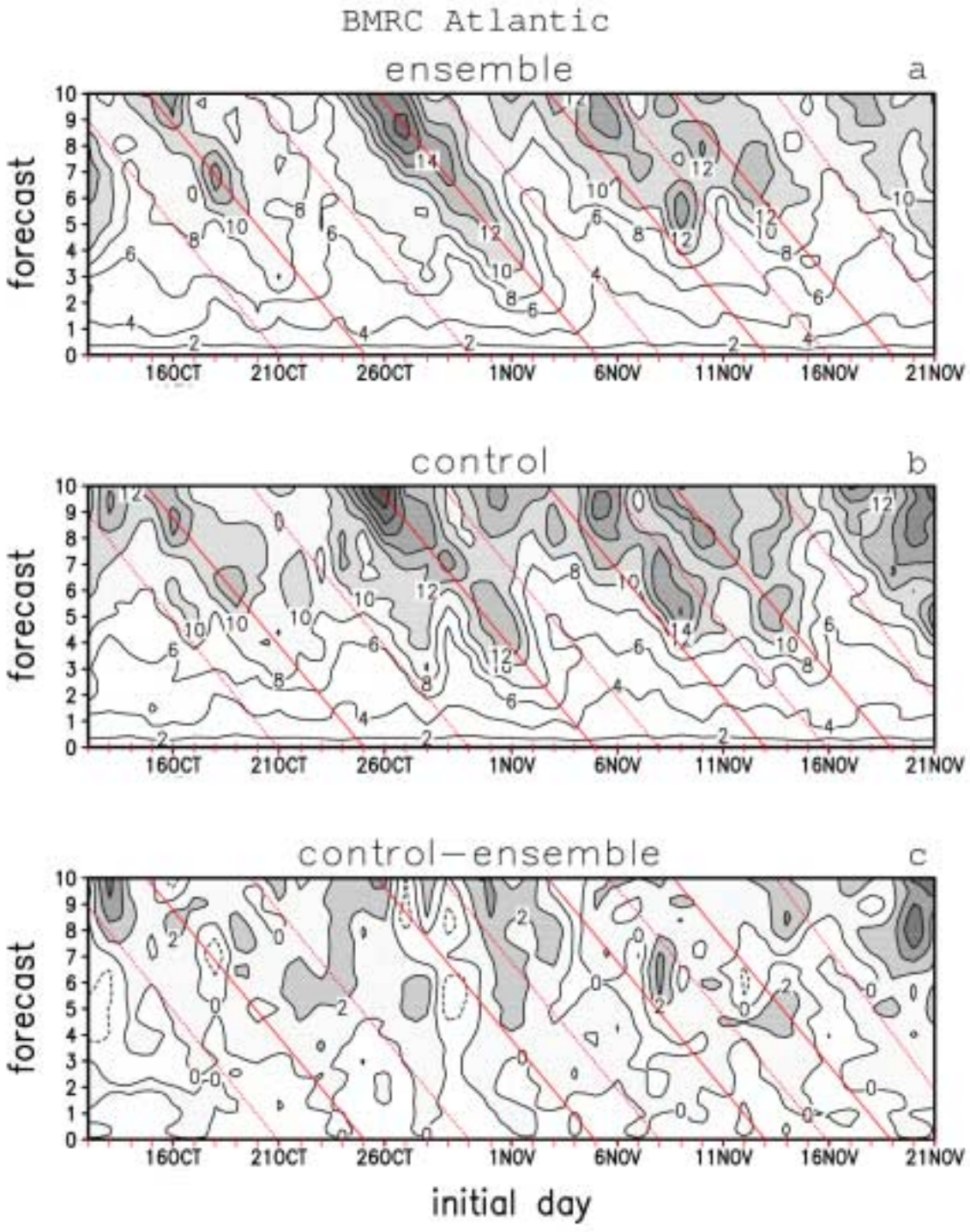

Figure 11 As in Figure 8 but for the North Atlantic sector.

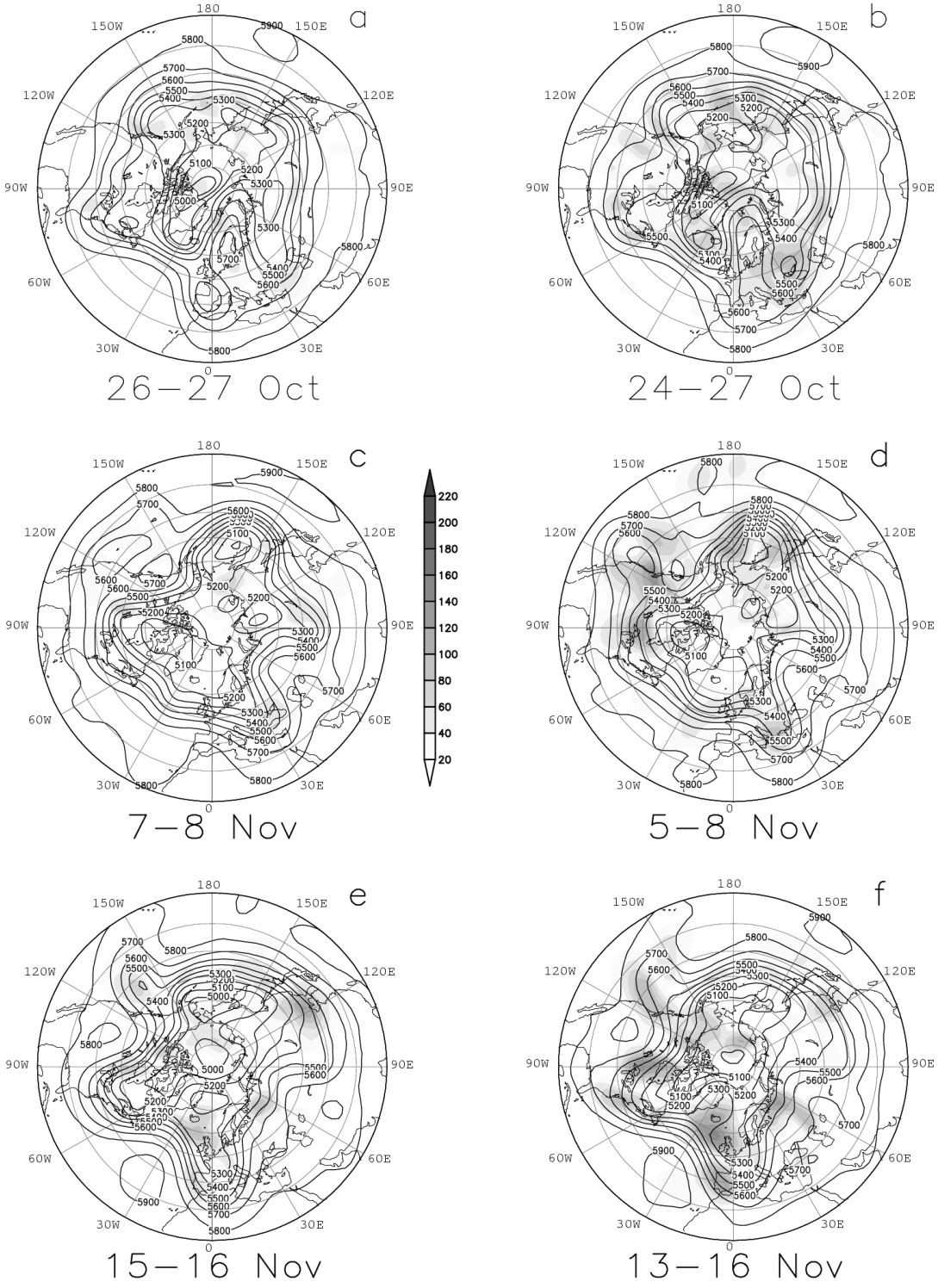

Figure 12 One and three day ensemble mean forecasts in the CSIRO model of Northern Hemisphere 500 hPa geopotential height (m) valid on 27 October, 8 November and 16 November 1979. Also shown in shading is the spread of the 16 ensemble members measured by the standard deviation about the ensemble mean.

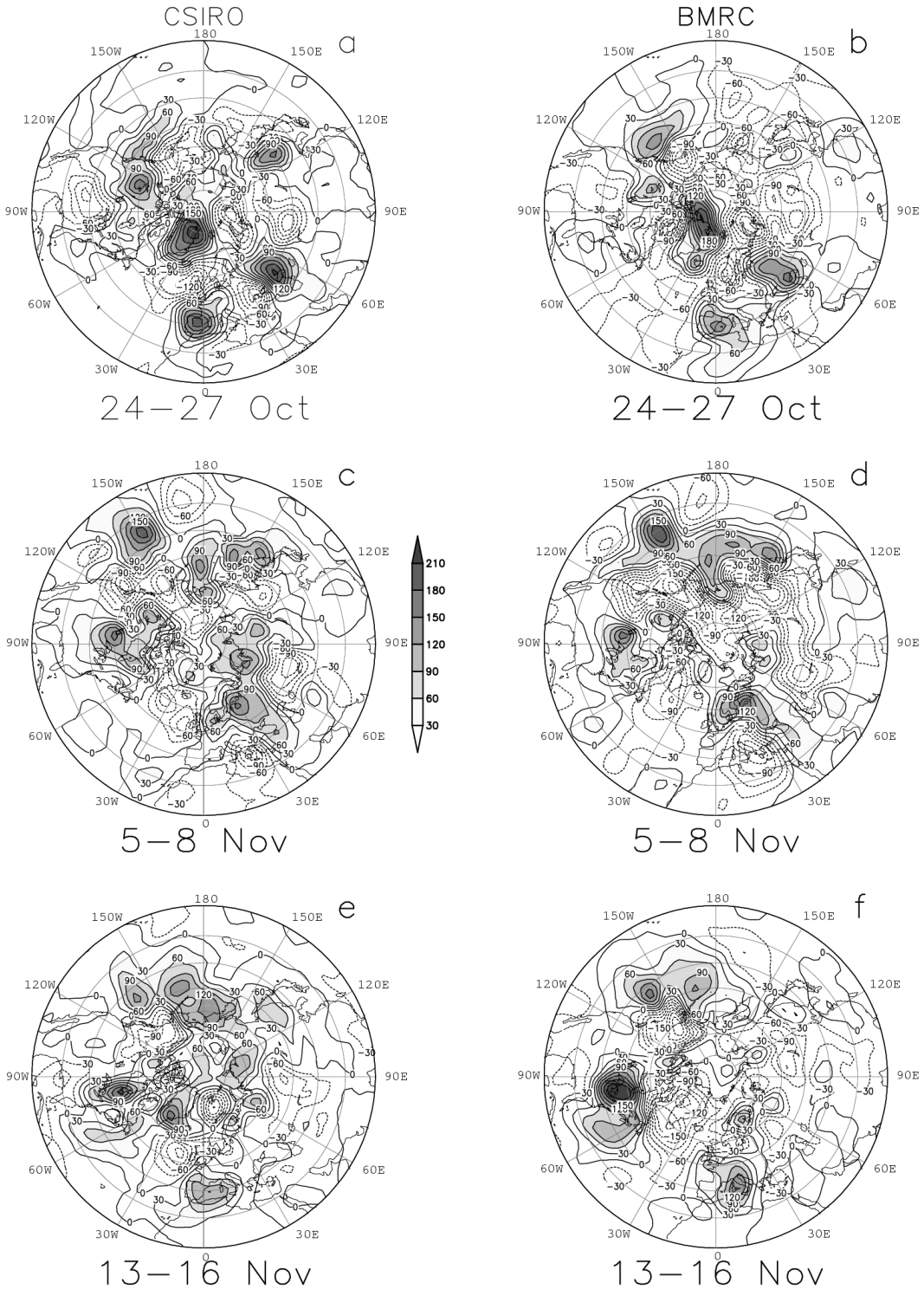

Figure 13 Horizontal structures of Northern Hemisphere 500 hPa geopotential height errors (m) in 3-day ensemble forecasts for the periods 24-27 October, 5-8 November and 13-16 November 1979 and for the CSIRO (left column) and BMRC (right column) models.

Figs 12c and d show 1 and 3-day ensemble mean forecasts respectively of 500 hPa geopotential height in the CSIRO GCM valid on 8 November 1979. We note that the 1-day forecast, in comparison with Fig.2a, is quite accurate in determining the high low blocking dipole structure in the Gulf of Alaska region. In contrast, in the 3-day forecast the dipole is of smaller scale and not yet fully cut-off from the westerly circulation. The standard deviations measuring the spread of the individual forecasts making up the ensemble are shown by the shading in Figs 12c and d. For the 3-day forecast, the peak spread occurs just downstream of the blocking region in the Gulf of Alaska, with subsidiary maxima both upstream and downstream. The errors, shown in Fig.13c at 3 days, and spread in the blocking region are consistent with the fact that the flow field over the Gulf of Alaska is a major region of fast growing instabilities as discussed in detail by Frederiksen (1997; Figs 1 and 2). We note from Fig.12d, and also evident in Fig.12c, that there is also a wave train of forecast variability associated with the Pacific jet stream; this again appears to be associated with baroclinic transients. There is also a region of significant spread associated with low intensification over Asia Minor and this is evident in both the 1- and 3-day forecasts. Here too there is a close correspondence between spread and error structure.

Figs 12e and f show 1- and 3-day ensemble mean forecasts respectively valid on 16 November 1979; again the 500 hPa heights are depicted and the results are based on the CSIRO GCM forecasts. The Atlantic block between Greenland and Scandinavia and the associated low over western Europe is captured by the 1-day forecast but more poorly represented in the 3-day forecast as seen from Figs 12e, f, 2c and the 3 day errors in Fig.13e. The spread of individual forecasts has maxima in the region of the Atlantic high-low blocking dipole. These results for errors and spread are also consistent with the instability calculations of Frederiksen (1997; Fig.3) which showed that fast growing instabilities were associated with the development of Atlantic block. Figs 12e and f show wave trains of forecast variability from the east coast of Asia across the Pacific which are associated with baroclinic transients in the major Pacific storm track. The close correspondence between spread and error structure is also evident for this period (Figs 12f and 13e).

We have also examined the structural organization of forecast variability and errors associated with the American blocking dipole (Fig.2d) that develops and matures around 22 to 23 November. Again 1- and 3-day ensemble forecasts with the CSIRO GCM have maxima of forecast spread in and around the region of formation of the high-low dipole with generally larger values for the 3-day forecasts (not shown).

The general relationships between errors, forecast variability and the formation of blocking dipoles shown in this section for the CSIRO GCM have also been found to be valid for forecasts based on the BMRC GCM using the ECMWF data set.

9 Conclusions

We have implemented and applied ensemble prediction methods based on fast growing perturbations within the CSIRO conformal-cubic and BMRC spectral general circulation models. The methodology employs an iterative procedure in which perturbations analogous to the leading (fastest growing) Lyapunov vector are obtained by a breeding method. We have used a procedure in which bred perturbations are generated over a 10-day period and thereafter ensemble (and control) forecasts are performed based on the bred perturbations and a subsequent self-breeding method. For the ensemble

forecasts, which have been performed every 12 hours and for 10 days ahead, we have used 16 paired perturbations of opposite signs generated from 8 independent breeding cycles.

In this study we have studied the performance of the ensemble prediction method, in comparison with single control forecasts, for initial conditions taken from the period between 0000 UTC on 11 October 1979 and 1200 UTC on 21 November 1979. We have focused on Northern Hemisphere flow during this period since it was a time of development, maturation and decay of large-scale blocks in the major blocking regions over Europe, over the Gulf of Alaska, over the North Atlantic Ocean and as well over North America. A major aim of our work has been to examine the variability of predictability depending on the particular synoptic situations, contrasting the growth, maturation and decay of blocks and alternating times of strong zonal flows. In order to establish that our findings are robust, and that large-scale forecast errors arise primarily from atmospheric instabilities rather than due to model deficiencies (Reynolds et al. 1994; Toth et al. 1997), we have compared results from the two different CSIRO and BMRC models and employing two different analysis data sets from NCEP and ECMWF.

Within a given model, the eight pairs of bred perturbations have been found to have similar large-scale features, while the stochasticity associated with the convection schemes introduce some differences from the expected leading Lyapunov vector structure. The bred perturbations are found to have large amplitudes in the regions of major instabilities. In particular during the growth of the Gulf of Alaska and North Atlantic blocks there are close similarities in the structures of the bred perturbations and the instabilities of Frederiksen (1997, 2000) in the blocking regions.

For both the CSIRO and BMRC models, on average the ensemble mean forecast is better than the control forecast for forecast times longer than 3 or 4 days. We have found that 500 hPa Northern Hemisphere RMS errors of zonal wind and geopotential height (and meridional velocity and temperature), averaged between 0000 UTC on 11 October and 1200 UTC on 21 November 1979, are lower for the ensemble forecasts than for the control forecasts. Despite the different model formulations, the average error growth curves in the two models are quite similar with the CSIRO model ensemble generally performing slightly better than for the lower resolution BMRC model.

We have found that there is considerably variability in the skill of both ensemble and control forecasts initiated twice daily and that this variability is related to particular synoptic events. In particular, at a given forecast lead time, errors tend to be larger for forecasts validating when blocks are developing or decaying and smaller for mature blocks. We have found that this is true both for Northern Hemisphere average errors and for errors averaged over 60° longitude sectors of the particular blocking regions. Similar results are also found for 60° longitude sectors upstream and downstream of the blocking regions and, in particular, we have focused on the Atlantic sector between 0° - 60°W. We note that these results are consistent with the notion that errors grow rapidly when dynamical development is rapid (Frederiksen and Bell 1990) and are suppressed in the presence of large-scale equivalent barotropic waves such as mature blocks (Frederiksen 1978; Colucci and Baumhefner 1992).

We have also studied the spread of ensemble member forecasts which provides a measure of their consistency and likely skill. We have examined the variability of error growth associated with different ensemble members. This has been done for errors averaged over the Northern Hemisphere extratropics and averaged over the Atlantic sector and as well the geographical distribution of the spread has been analysed for the major blocking events. We have found that forecast variability is particularly

associated with rapidly developing systems such as baroclinic transients in the storm tracks and developing blocks. The rapidly growing errors and forecast spread in the regions of block development are consistent with the fast growing instabilities that occur there (Frederiksen and Bell 1990; Frederiksen 1997, 2000).

We have found that the use of an ensemble forecasting approach, based on an iterative breeding method, generally improves forecast skill including during blocking events. Furthermore, at timescales beyond 4 days, it is possible to extend the range of ensemble mean forecasts by an extra half or one day beyond control forecasts with the same skill.

10 Acknowledgments

It is a pleasure to thank Martin Dix, Jack Katzfey and John McGregor for assistance in using the CSIRO conformal-cubic atmospheric circulation model and pre- and post-processing software. We wish to thank Mike Manton for making available the BMRC spectral atmospheric circulation model for this study.

11 References

Anderson, J.L., The climatology of blocking in a numerical forecast model. *J. Climate*, **6**, 1041-1056, 1993.

Anderson, J.L., Selection of initial conditions for ensemble forecasts in a simple perfect model framework. *J. Atmos. Sci*., **53**, 22-36, 1996.

Bengtsson, L., Numerical prediction of atmospheric blocking: A case study. *Tellus*, **33**, 19-24, 1981.

Borges, M.D. and D. L. Hartmann, Barotropic instability and optimal perturbations of observed nonzonal flows. *J.Atmos.Sci.*, 49, 335-354, 1992.

Colucci, S.J. and D. P. Baumhefner, Initial weather regimes as predictors of numerical 30-day mean forecast accuracy. *J. Atmos. Sci*., **49**, 1652-1671, 1992.

de Pondeca, M.S.F.A., A. Barcilon, and X. Zou, An adjoint sensitivity study of the efficacy of modal and nonmodal perturbations in causing model block onset. *J. Atmos. Sci*., **55**, 2095-2118, 1998a.

de Pondeca, M.S.F.A., A. Barcilon, and X. Zou, The role of wave breaking, linear instability, and PV transports in model block onset. *J. Atmos. Sci*., **55**, 2852-2873, 1998b.

Frederiksen, J.S., Instability of planetary waves and zonal flows in two-layer models on a sphere. *Quart. J. Roy. Meteor. Soc*., **104**, 841-872. 1978.

Frederiksen, J.S., A unified three-dimensional instability theory of the onset of blocking and cyclogensis. *J.Atmos.Sci.*, **39**, 969-982, 1982.

Frederiksen, J.S., A unified three-dimensional instability theory of the onset of blocking and cyclogenesis. II Teleconnection Patterns. *J. Atmos. Sci*., **40**, 2593-2609, 1983.

Frederiksen, J.S., Adjoint sensitivity and finite-time normal mode disturbances during blocking. *J. Atmos. Sci*., **54**, 1144-1165, 1997.

Frederiksen, J.S., Precursors to blocking anomalies: The tangent linear and inverse problems. *J.Atmos.Sci.*, **55** 2419-2436, 1998.

Frederiksen, J. S., Subgrid-scale parameterizations of eddy-topographic force, eddy viscosity and stochastic backscatter for flow over topography. *J. Atmos. Sci*., **56**, 1481-1494, 1999.

Frederiksen, J.S., Singular vectors, finite-time normal modes and error growth during blocking. *J. Atmos. Sci*., **57**, 312-333, 2000.

Frederiksen, J.S., and R. C. Bell, North Atlantic blocking during January 1979: Linear theory. *Quart. J. Roy. Meteor. Soc*., 116, 1289-1313, 1990.

Frederiksen, J.S., M. R. Dix, and S. Kepert, Systematic energy errors and the tendency toward canonical equilibrium in atmospheric circulation models. *J. Atmos. Sci*., **53**, 887-904, 1996.

Hart, T.L., Bourke, W., McAvaney, B.J., Forgan, W. and J.L. McGregor, Atmospheric general circulation simulations with the BMRC global spectral model: The impact of revised physical parmeterizations. *J.Climate*, **3**, 436-459, 1990.

Houtekamer, P.L., L.Lefaivre, J.Derome, H.Ritchie and H.L.Mitchell, A system simulation approach to ensemble prediction. *Mon. Wea. Rev*., **124**, 1225-1242, 1996.

Kalnay, E., Atmospheric modeling, data assimilation and predictability, Cambridge University Press, in press, 2002.

Kimoto, M., H. Mukougawa, and S. Yoden, Medium-range forecast skill variation and blocking transition: A case study. *Mon.Wea.Rev.*, **120** 1616-1627, 1992.

Leith, C.E., Theoretical skill of Monte Carlo forecasts. *Mon.Wea.Rev.*, **102**, 409-418, 1974.

Li, Z., A. Barcilon and I.M. Navon, Study of block onset using sensitivity perturbations in climatological flows. *Mon.Wea.Rev.* **127**, 879-900, 1999.

McGregor, J.L. and M.R. Dix, The CSIRO conformal-cubic atmospheric GCM. In: IUTAM symposium on Advances in Mathematical Modelling of Atmosphere and Ocean Dynamics, 298 pp. Ed. P.F. Hodnett. Kluwer Academic Publishers, Dordrecht, 197-202, 2001.

Molteni, F., R. Buizza, T. Palmer, and T. Petroliagis, The ECMWF ensemble prediction system: Methodology and validation. *Quart. J. Roy. Meteor. Soc*., **122**, 73-119, 1996.

Noar, P.F., Numerical modelling of blocking with reference to June 1982. *Aust.Meteor.Mag.*, **31**, 37-49, 1983.

Noone, D., and I. Simmonds, Similarity of 'fast-growing perturbations' and an illustrative experiment with ensemble forecasting. *Aust. Meteor. Mag*., **47**, 5-19, 1998.

O'Kane, T.J., and J.S. Frederiksen, Integro-differential closure equations for inhomogeneous turbulence. *ANZIAM J.*, 2002 (In press).

Palmer, T.N., R. Gelaro, J. Barkmeijer, and R. Buizza, Singular vectors, metrics, and adaptive observations. *J. Atmos. Sci*. **55**, 633-653, 1998.

Reynolds, C.A., Webster, P.J. and E. Kalnay, Random error growth in NMC's global forecasts. *Mon.Wea.Rev.*, **122**, 1281-1305, 1994.

Simmons, A.J., J. M. Wallace, and G. W. Branstator, Barotropic wave propagations and instability, and atmospheric teleconnection patterns. *J. Atmos. Sci*., **40**, 1363-1392, 1983.

Smagorinsky, J., Manabe, S., and J.L. Holloway, Numerical results from a nine-level general circulation model of the atmosphere. *Mon.Wea.Rev.*, **93**, 727-768, 1965.

Szunyogh, I., E. Kalnay, and Z. Toth, A comparison of Lyapunov and Optimal vectors in a low-resolution GCM. *Tellus*, **48A**, 200-227, 1997.

Tibaldi, S., P. Ruti, and M. Maruca, Operational predictability of winter blocking at ECMWF: an update. *Ann. Geophysicae*, **13**, 305-317, 1995.

Toth, Z., and E. Kalnay, Ensemble forecasting at NMC: the generation of perturbations. *Bull. Amer. Meteor. Soc*., **174**, 2317-2330, 1993.

Toth, Z., and E. Kalnay, Ensemble forecasting at NCEP and the breeding method. *Mon.Wea.Rev.*, **125**, 3297-3319, 1997.

Toth, Z., Kalnay, E., Tracton, S.M., Wobus, R., and J. Irwin, 1997. A synoptic evaluation of the NCEP ensemble. *Weather and Forecasting*, **12**, 140-155, 1997.

CSIRO Atmospheric Research Technical Papers

CSIRO Atmospheric Research Technical Papers are thoroughly reviewed reports that document significant scientific achievements such as model development and results from field observations. Typically, Technical Papers contain material that is too detailed or specialised for publication in a scientific journal.

From July 2000, all new Technical Papers will appear on our Web site; some of these Technical Papers may also appear in paper form.

CSIRO Atmospheric Research Technical Papers may be issued out of sequence.

CSIRO Atmospheric Research Technical Papers: ISSN 1445-6982

Complete list

(Series title changed from CSIRO Division of Atmospheric Research Technical Papers at number 38)

No. 1 Galbally, I.E.; Roy, C.R.; O'Brien, R.S.; Ridley, B.A.; Hastie, D.R.; Evans, W.J.F.; McElroy, C.T.; Kerr, J.B.; Hyson, P.; Knight, W.; Laby, J.E.
Measurements of trace composition of the Austral stratosphere: chemical and meteorological data. 1983. 31 p.

No. 2 Enting, I.G.
Error analysis for parameter estimates from constrained inversion. 1983. 18 p.

No. 3 Enting, I.G.; Pearman, G.I.
Refinements to a one-dimensional carbon cycle model. 1983. 35 p.

No. 4 Francey, R.J.; Barbetti, M.; Bird, T.; Beardsmore, D.; Coupland, W.; Dolezal, J.E.; Farquhar, G.D.; Flynn, R.G.; Fraser, P.J.; Gifford, R.M.; Goodman, H.S.; Kunda, B.; McPhail, S.; Nanson, G.; Pearman, G.I.; Richards, N.G.; Sharkey, T.D.; Temple, R.B.; Weir, B.
Isotopes in tree rings. 1984. 86 p.

No. 5 Enting, I.G.
Techniques for determining surface sources from surface observations of atmospheric constituents. 1984. 30 p.

No. 6 Beardsmore, D.J.; Pearman, G.I.; O'Brien, R.C.
The CSIRO (Australia) Atmospheric Carbon Dioxide Monitoring Program: surface data. 1984. 115 p.

No. 7 Scott, J.C.
High speed magnetic tape interface for a microcomputer. 1984. 17 p.

No. 8 Galbally, I.E.; Roy, C.R.; Elsworth, C.M.; Rabich, H.A.H.
The measurement of nitrogen oxide (NO, NO2) exchange over plant/soil surfaces. 1985. 23 p.

No. 9 Enting, I.G.
A strategy for calibrating atmospheric transport models. 1985. 25 p.

No. 10 O'Brien, D.M.
TOVPIX: software for extraction and calibration of TOVS data from the high resolution picture transmission from TIROS-N satellites. 1985. 41 p.

No. 11 Enting, I.G.; Mansbridge, J.V.
Description of a two-dimensional atmospheric transport model. 1986. 22 p.

No. 12 Everett, J.R.; O'Brien, D.M.; Davis, T.J.
A report on experiments to measure average fibre diameters by optical fourier analysis. 1986. 22 p.

No. 13 Enting, I.G.
A signal processing approach to analysing background atmospheric constituent data. 1986. 21 p.

No. 14 Enting, I.G.; Mansbridge, J.V.
Preliminary studies with a two- dimensional model using transport fields derived from a GCM. 1987. 47 p.

No. 15 O'Brien, D.M.; Mitchell, R.M.
Technical assessment of the joint CSIRO/Bureau of Meteorology proposal for a geostationary imager/ sounder over the Australian region. 1987. 53 p.

No. 16 Galbally, I.E.; Manins, P.C.; Ripari, L.; Bateup, R.
A numerical model of the late (ascending) stage of a nuclear fireball. 1987. 89 p.

No. 17 Durre, A.M.; Beer, T.
Wind information prediction study: Annaburroo meteorological data analysis. 1989. 30 p. + diskette.

No. 18 Mansbridge, J.V.; Enting, I.G.
Sensitivity studies in a two- dimensional atmospheric transport model. 1989. 33 p.

No. 19 O'Brien, D.M.; Mitchell, R.M.
Zones of feasibility for retrieval of surface pressure from observations of absorption in the A band of oxygen. 1989. 12 p.

No. 20 Evans, J.L.
Envisaged impacts of enhanced greenhouse warming on tropical cyclones in the Australian region. 1990. 31 p. [Out of print]

No. 21 Whetton, P.H.; Pittock, A.B.
Australian region intercomparison of the results of some general circulation models used in enhanced greenhouse experiments. 1991. 73 p. [Out of print]

No. 22 Enting, I.G.
Calculating future atmospheric CO2 concentrations. 1991. 32 p. available electronically

No. 23 Kowalczyk, E.A.; Garratt, J.R.; Krummel, P.B.
A soil-canopy scheme for use in a numerical model of the atmosphere — 1D stand- alone model. 1992. 56 p.

No. 24 Physick, W.L.; Noonan, J.A.; McGregor, J.L.; Hurley, P.J.; Abbs, D.J.; Manins, P.C.
LADM: A Lagrangian Atmospheric Dispersion Model. 1994. 137 p.

No. 25 Enting, I.G.
Constraining the atmospheric carbon budget: a preliminary assessment. 1992. 28 p. Available electronically

No. 26 McGregor, J.L.; Gordon, H.B.; Watterson, I.G.; Dix, M.R.; Rotstayn, L.D.
The CSIRO 9-level atmospheric general circulation model. 1993. 89 p.

No. 27 Enting, I.G.; Lassey, K.R.
Projections of future CO2. with appendix by R.A. Houghton. 1993. 42 p. Available electronically

No. 28 [Not published]

No. 29 Enting, I.G.; Trudinger, C.M.; Francey, R.J.; Granek, H.
Synthesis inversion of atmospheric CO2 using the GISS tracer transport model. 1993. 44 p.

No. 30 O'Brien, D.M.
Radiation fluxes and cloud amounts predicted by the CSIRO nine level GCM and observed by ERBE and ISCCP. 1993. 37 p.

No. 31 Enting, I.G.; Wigley, T.M.L.; Heimann, M.
Future emissions and concentrations of carbon dioxide: key ocean/atmosphere/land analyses. 1994. 120 p. available electronically

No. 32 Kowalczyk, E.A.; Garratt, J.R.; Krummel, P.B.
Implementation of a soil-canopy scheme into the CSIRO GCM — regional aspects of the model response. 1994. 59 p.

No. 33 Prata, A.J.
Validation data for land surface temperature determination from satellites. 1994. 40 p.

No. 34 Dilley, A.C.; Elsum, C.C.
Improved AVHRR data navigation using automated land feature recognition to correct a satellite orbital model. 1994. 22 p.

No. 35 Hill, R.H.; Long, A.B.
The CSIRO dual-frequency microwave radiometer. 1995. 16 p.

No. 36 Rayner, P.J.; Law, R.M.
A comparison of modelled responses to prescribed CO2 sources. 1995. 84 p.

No. 37 Hennessy, K.J.
CSIRO Climate change output. 1998. 23 p.

No. 38 Enting, I. G.
Attribution of greenhouse gas emissions, concentrations and radiative forcing. 1998. 29 p. Available electronically

No. 39 O'Brien, D.M.; Tregoning, P..
Geographical distributions of occultations of GPS satellites viewed from a low earth orbiting satellite. 1998. 23 p.

No. 40 Enting, I.G.
Characterising the temporal variability of the global carbon cycle. 1999. 23 p. Available electronically

No. 41 Enting, I.G. and Law, R.M.
Characteristing Historical Responsibility for the Greenhouse Effect, 2002. 50 p. Electronic edition only

No. 42 Mitchell, R.M.
Calibration status of the NOAA AVHRR solar reflectance channels: CalWatch revision 1. 1999. 20 p.

No. 43 Hurley, P.J.
The Air Pollution Model (TAPM) Version 1: technical description and examples. 1999. 41 p. Available electronically

No. 44 Frederiksen, J.S.; Dix, M.R.; Davies, A.G.
A new eddy diffusion parameterisation for the CSIRO GCM. 2000. 31 p.

No. 45 Young, S.A.
Vegetation canopy lidar studies. 2000. 35 p. Electronic edition only.

No. 46 Prata, A.J.
Global Distribution of Maximum Land Surface Temperature Inferred from Satellites: Implications for the Advanced Along Tracking Scan Radiometer. 2000. 30 p. Electronic edition only.

No. 47 Prata, A.J.
Precipitable water retrieval from multi-filtered shadowband radiometer measurements. 2000. 14 p. Electronic edition only.

No. 48 Prata, A.J., Grant, I.F.
Determination of mass loadings and plume heights of volcanic ash clouds from satellite data. 2001. 39 p. Electronic edition only.

No. 49 O'Brien, D.M.
Numerical calculation of the transfer of polarized radiation by a scattering and absorbing atmosphere. 2001. 65 p. Electronic edition only.

No. 50 R.L. Law, Vohralik, P.F.
Methane sources from mass-balance inversions: Sensitivity to transport. 2001 27p. Electronic edition only.

No. 51 Meyer, C.P., Galbally, I.E., Wang, Y.P., Weeks, I.A., Jamie, I., Griffith, D.W.T.,
Two automatic chamber techniques for measuring soil-atmosphere exchanges of trace gases and results of their use in the OASIS field experiment. 2001 33 p. Electronic edition only.

No. 52 Mitchell, R.M. In-flight characteristics of the space count of NOAA AVHRR channels 1 and 2. 201 24 p. Electronic edition only.

No. 53 Young, S.A. An investigation into the performance of algorithms used to retrieve cloud parameters from LITE lidar data, and implications for their use with PICASSO-CENA lidar data. Electronic edition only.

No 54 [In preparation]

No.55 Hurley, P. The Air Pollution Model (TAPM) Version 2. Part 1. Technical Description. Electronic edition only.

No. 56 Enting, I.G. and Trudinger C.M.
Modelling earth system change. 1, Validating parameterisations for attribution calculations. Electronic edition only.

No.57 Hurley, P., Physick, W.L. and Luhar, A.K. The Air Pollution Model (TAPM) Version 2. Part 2. Summary of some verification studies.
Electronic edition only.